ABOUT RESEARCH PROGRAMS AT THE RADIO TELESCOPE "URAN-4" IRA NASU – MONITORING OF FLUXES OF POWERFUL RADIO SOURCES, STUDY OF THE SUN'S SUPERCORONA, OBSERVATIONS OF SOLAR ECLIPSE

A.L. Sukharev, M.I. Ryabov, V.V. Galanin, V.G. Komendant

Odessa observatory "URAN-4" Institute of Radio Astronomy of the National Academy of Sciences of Ukraine (IRA NASU)

ABSTRACT. During 2020–2023, an initiative series of observation programs was carried out on a radiometer designed and manufactured by V.V. Galanin. Among them are observations of ionospheric scintillations of powerful radio sources Cas A, Cyg A, Vir A, Tau A, Per A, on the URAN-4 radio telescope (IRA NASU) at frequencies of 20 and 25 MHz. The observations were carried out at various states of Solar and geomagnetic activity and allow us to analyze the response of the ionosphere in the region of the Odessa Magnetic Anomaly to disturbing events. It was found that the radio source 3C 84 (Per A) is the least noisy at the location of the URAN-4 antenna and is well suited for studying the ionospheric response during magnetic storms. The recorded scintillation periods of the studied radio sources, on "calm" days, are in the range of 1-2 minutes. During magnetic storms, the periods of scintillations are reduced to 10-30 seconds. The paper considers the features of the response of scintillations of different radio sources to a magnetic storm, since they shine through different spatial regions of the ionosphere. Of particular interest are observations of the radio source Tau A (3C 144), which annually, in June, shines through the Solar Supercorona. Processing scans of such observations of the 3C 144 source shows an increase flux variations with an average "period" of about 5-10 seconds. Observations were also made to record the features of radio background variations during partial Solar eclipse. It is shown that during a Solar eclipse, the level of background radio noise increases significantly. At the same time, the background level on the next day after the eclipse was still quite high. A more detailed analysis of this effect is planned and, if possible, repeated observations.

Keywords: ionospheric scintillations, radio sources, antenna array, geomagnetic variations, magnetic anomaly

АНОТАЦІЯ. Протягом 2020 – 2023 років, було виконано ініціативну серію програм спостережень на радіометрі, спроектованому та виготовленому В.В. Галаніним. Серед них спостереження іоносферних мерехтінь потужних радіоджерел Cas A, Cyg A, Virg A, Tau A, Pers A, на радіотелескопі URAN-4 (IRA NASU) на частотах 20 і 25 МГц. Спостереження проводилися за різних станів сонячної та геомагнітної активності та дозволяють аналізувати відгук іоносфери в регіоні Одеської Магнітної Аномалії на обурюючі події. Було встановлено, що радіоджерело 3C 84 (Perseus A) є найменш зашумленим, у місці розташування антени URAN-4 і добре підходить для вивчення іоносферного відгуку під час магнітних бур. Реєстровані періоди мерехтіння досліджуваних радіоджерел, у «спокійні» дні, перебувають у інтервалі 1-2 хвилини. Під час магнітних бур, періоди мерехтіння зменшуються до 10-30 секунд. У роботі розглянуто особливості відгуку мерехтінь різних джерел на магнітну бурю, оскільки вони просвічують різні просторові області іоносфери. Особливий інтерес становлять спостереження радіоджерела Taurus A (3C 144), який щорічно, у червні, просвічує надкорону Сонця. Обробка сканів таких спостережень джерела 3C 144 показує посилення варіацій із середнім «періодом» близько 5-10 секунд. Також було проведено спостереження щодо реєстрації особливостей варіацій радіофону під час часткового Сонячного затемнення. Показано, що під час Сонячного затемнення рівень фонового радіо-шуму значно підвищується. При цьому рівень фону наступного дня після затемнення був досить високим. Планується докладніший аналіз цього ефекту за наявності можливостей проведення повторних спостережень.

Ключові слова: іоносферні мерехтіння, радіоджерела, антенна решітка, геомагнітні варіації, магнітна аномалія.

1. Introduction

During the development of the anomalous 25th solar cycle (beginning in December 2019), the most important task is to study the ionospheric response to extreme manifestations of solar and geomagnetic activity. One of the most scientifically based and widely used methods for studying the Earth's ionosphere and the effects of space weather manifestations is the method of ionospheric scintillations of discrete space radio sources [1, 2]. The main contribution to the scintillations of signals from discrete radio sources is made by inhomogeneities, with transverse dimensions to the line of sight, of order of size the Fresnel zone: $\Lambda_{fr} = \sqrt{\lambda r}$, where λ – wavelength, and r – distance to the scattering layer. These

inhomogeneities focus or defocus signals from cosmic radio sources. At the same time, extended radio sources with angular dimensions θ which exceed the angular size of the Fresnel zone $\theta_{fr} = \Lambda_{fr}/r \sim \sqrt{\lambda/r}$ will not have scintillations, because the addition of oscillations coming to the observation point from different areas of these sources will be incoherent [3, 4]. Ionospheric scintillations strongly depend on the state of the Earth's ionosphere and magnetosphere under the influence of solar activity, and therefore are excellent indicators of space weather. Although this method has been used since the 1950s, many unresolved questions remain. These include the connection between ionospheric scintillation and geomagnetic pulsations, as well as the connection between ionospheric scintillation and variations in cosmic ray fluxes. In addition, the influence of large regional magnetic anomalies on the ionospheric response during extreme space weather events is poorly understood. This work uses data from the URAN-4 (IRA NASU) low frequency radio telescope, operating in the 10-30 MHz range. A unique feature of this radio telescope is its location near the Odessa regional geomagnetic anomaly. The dome of the anomalous field of this anomaly, according to satellite data, extends to ionospheric heights, which makes it possible to study its response to solar activity [5].

2. Brief description of the low-frequency radio telescope URAN-4 and processing observational data

The low-frequency decameter radio telescope, URAN-4 (operated by the Institute of Radio Astronomy of the National Academy of Sciences of Ukraine (IRA NASU)) (began observations in 1987) is a phased array with electronic control of the antenna beam direction. The antenna consists of 128 pairs of vibrators located on an area the size 232.5 x 22.5 meters and oriented in the east-west direction. Thus, the antenna receives a signal in two linear polarizations A and B. The antenna beam pattern has the size 2.7° x 22° at a frequency of 25 MHz. URAN-4 is one of the elements of the national low-frequency radio interferometric system URAN, Ukraine. In very-long-baseline interferometer mode, the angular resolution reaches 2 arcseconds. The sensitivity with a frequency bandwidth of 14 kHz is 100 Jy (and in interferometer mode – 10 Jy) at a frequency of 25 MHz [42]. The hardware complex includes an upgraded antenna control device and a radiometer for recording radio emissions, which was developed and constructed by IRA NASU researcher Valery Galanin. This device controls discrete movement of the antenna's beam pattern when observing radio sources and sets the required observation mode. Currently, observations are carried out at frequencies of 20 and 25 MHz. The radiometer operates in various modes: full power, modulation mode, average power, using the telescope design in the form of two halves of the antenna. The radiometer is made on an ATMEL AT90S8515 microcontroller with a communication circuit with a control computer. The REGICEA software for antenna control and observation planning was written in the Delphi programming language. The resulting observation file contains the time in Julian dates, the total power (P) and the differences between the two halves of

the antenna (M). The main operating mode is modulation ($P-M$). In modulation mode, random uncorrelated noise is suppressed and the noise track of the signal is significantly reduced, which is especially important when observing weak sources (for example, 3C 84). Figure 1 shows an example of recording in modulation mode for the 3C 405 source and in full power mode for the 3C 461 source. The program for monitoring fluxes of powerful radio sources was started on the initiative of the authors (M.I. Ryabov and V.V. Galanin) from the moment of commissioning the URAN-4 radio telescope continues in present time.

Monitoring fluxes of radio sources and their scintillations is carried out in the mode of multiple passage of radio sources through the antenna's beam pattern. Supernova remnant 3C 144 (Taurus A) and radio galaxy 3C 274 (Virgo A) were recorded in the hour angle interval from -120m to +120m with a step of 40 min (7 scans in total). Radio galaxy 3C 405 was recorded in the interval of hour angles from -120m to +80m with a step of 40 min (6 scans in total). The most powerful radio source in the northern sky in the decameter range, supernova remnant 3C 461 (Cassiopeia A) was recorded in the hour angle interval from -60 m +120m with a step of 60 min (4 scans in total). Thus, the total monitoring time was 13 hours 20 minutes. And as a result of this 36-year monitoring, important data were obtained on seasonal-diurnal variations in the fluxes of radio sources and their scintillations over a period of 22–25 solar cycles [6, 7].

The main objects for studying ionospheric scintillations are the powerful radio galaxies 3C 274 (Virgo A), 3C 405 (Cygnus A), 3C 84 (Perseus A), as well as the remnants of supernova explosions 3C 461 (Cassiopeia A) and 3C 144 (Taurus A). Over 36 years of observations on the URAN-4, unique observational material was obtained on changes in the fluxes of radio sources and their scintillations during different cycles of solar and geomagnetic activity in the region of the Odessa magnetic anomaly.

Radio fluxes from space sources are written to the output file as relative values, in decibels (dB), relative to a highly stable noise generator (calibrated in antenna temperatures in Kelvin (K)). The amplitudes of the calibration steps were selected experimentally for each radio source in the sample.

Figure 2 shows a typical view of recording fragments of radio sources 3C 405 and 3C 144 (sequential passage through the antenna's beam pattern) on URAN-4. This allows us to immediately see the features, similarities and differences in the ionospheric responses to bursts of solar and geomagnetic activity for the entire sample of analyzed sources, on the final flux record.

The sampling rate in the output data file with records the sum and difference of the signals from two halves of the antenna, at frequencies 20 and 25 MHz, is 1 Hz (1 measurement per second). As can be seen from previous figures, ionospheric scintillation is superimposed on the sinusoidal trend from the registration of the antenna's beam pattern scans radio source. To isolate ionospheric scintillations, a semi-automatic method of data preprocessing and subsequent construction of digital dynamic spectra (using Short-Time Fourier Transform
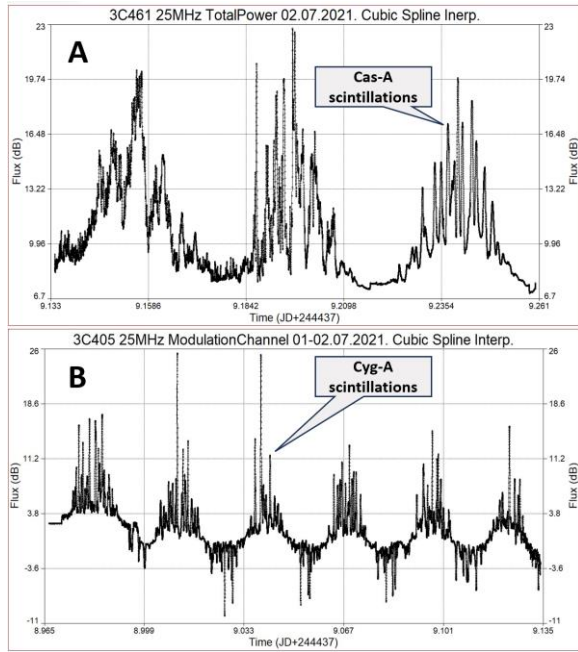
Figure 1: Examples of source scan records: A) 3C 461, frequency 25 MHz, full power with cubic smoothing spline interpolation; B) 3C 405, frequency 25 MHz, modulation mode with cubic smoothing spline interpolation. Records received 1-2 Jul 2021.
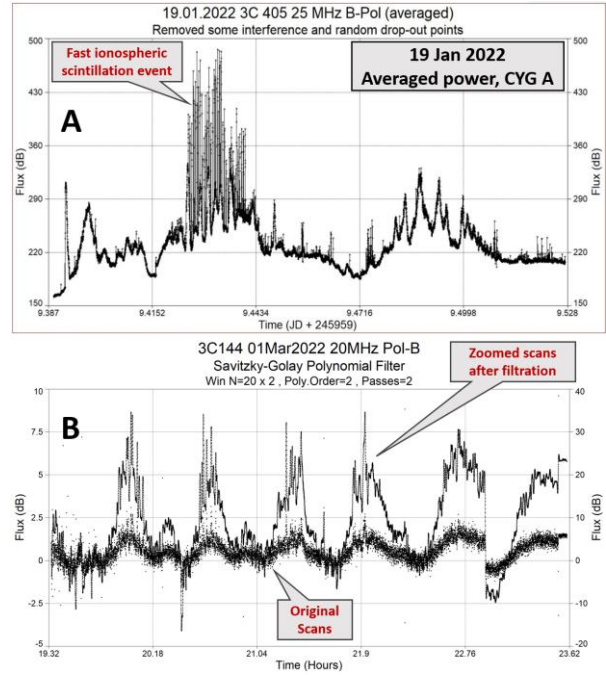

Figure 2: The figure shows: A) An example of a recording (Jan 19, 2022) of average power (the average value of the sum and difference signals of the half-antennas) for the radio source 3C 405 (frequency 25 MHz, linear polarization B). The average power graph has wider scan peaks, which is useful when recording scintillations, but is suitable for high-power sources. This example shows a scintillations burst with a characteristic time of about a minute; B) Example of original and smoothed recordings (Mar 1, 2022) modulation mode, for source 3C 144 (frequency 20 MHz, linear polarization B). Savitzky-Golay filter was used for smoothing [8] (graphs are shifted relative to each other for better visibility).

(STFT) and fast continuous wavelet transform methods) was developed and implemented. Due to the complex interference environment in the decameter range, the antenna's beam pattern (which under normal conditions is well described by the function *sin (x)/x*) is deformed. Under such conditions, data preprocessing consists of the following steps:

1) removal of the strongest radio interference and random outliers (manually).

2) smoothing the recording of radio source scans using three different approaches depending on the level of data noise. For low-noisy data, the Savitzky-Golay filter was used (most often for sources 3C 461 and 3C 84); when the noise was high enough, with weak impulse noise, data interpolation using a smoothing cubic spline with cross-validation was used, where smoothing level is automatically determined using procedure so-called cross-validation [9] (usually for sources 3C 405 and 3C 274). This method allows us to draw scans of radio sources and variations in the radio flux even in the case of noise bursts caused by interference during tens of minutes. In the case of strong continuous noise, which is often recorded in the direction of the 3C 144 source, the Loess method (Locally estimated scatterplot smoothing) implementation of the locally-weighted least-squares procedure with Gaussian weighting function was used [10]. This method can isolate scintillations in the presence of fairly long-term interference, which is not uncommon at the URAN-4 location, and was most often used for observations of 3C 144, since the noise in the direction of this source is often greater than for the rest of the sources in the sample.

3) Since ionospheric scintillations are superimposed on the sinusoidal trend, the trend is removed to isolate them and subsequent analysis. This is complicated by the fact that the main shape of scans of radio sources often differs from the theoretical one due to radio-interference. In this work, the main method for identifying scintillations was FFT filtering with a Hamming spectral window [11]. Spectral windowing is used to reduce spectrum leakage so that components in low spectral power data can be selected and recovered. Thus, even weak scintillations can be clearly distinguished from a noisy background. The Hamming spectral window does not completely attenuate to zero at the edges of the rolloff, and typically the filter can recover the full range of data with 1% edge effects at the beginning and end of the data series. An example of FFT filtering is shown in Figure 3.

Despite the relative simplicity and effectiveness of the FFT band-pass filtering method, in some cases it can leave a small false wave in the data, which can be noticeable on days with no or weak scintillation. Therefore, in 2023, the decomposition of observational data into individual quasiperiodic and noise-like components by the Caterpillar-SSA method began to be used (more details about this method are described in the work [12]), which made it possible to significantly eliminate distortions from filtering in recordings of weak scintillations.
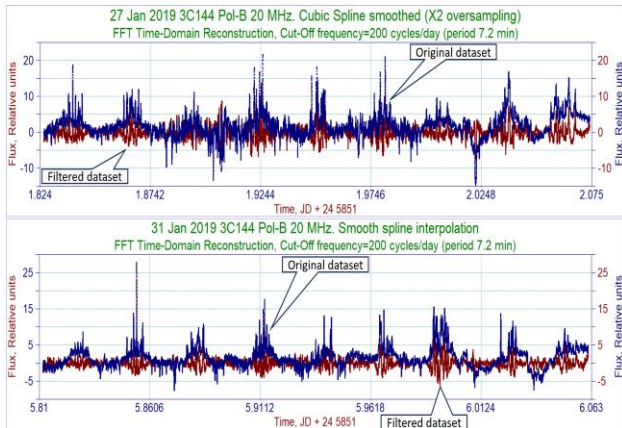
Figure 3: Initial and FFT-filtered data from radio source 3C 144 (frequency 20 MHz, linear polarization B), such that the time scale varies less than 7 minutes (cutoff frequency 200 cycles/day). Top panel – record 27 Jan 2019, bottom panel – record 31 Jan 2019.
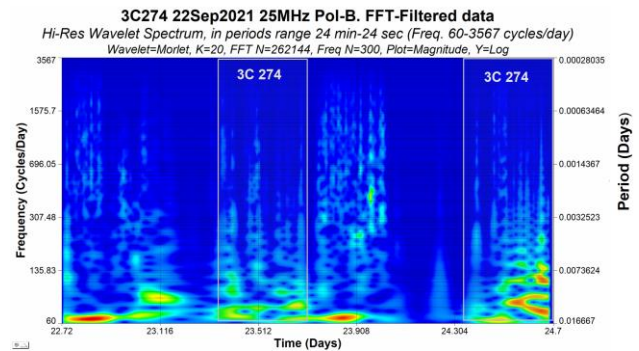

Figure 4: An example of a wavelet spectrogram (frequency 25 MHz, polarization B, period band from 24 seconds to 24 minutes) of the development of ionospheric scintillations during sequential recording of a sample of radio sources in the time interval 22-24 Sep 2021, during weak geomagnetic disturbances. In the graph, source 3C 274 is highlighted by rectangles. The change in noise and quasi-harmonic components of variability is clearly visible; as the time scale decreases, variations in the radio flux become completely noise. Quasi-harmonic variations here are concentrated mainly in a band of periods 10-20 minutes.

4) Finally, after the above-described pre-processing of the data and their normalization, spectrograms were constructed. In low-frequency astronomy, standard practice for this is to use the STFT method (for example [13]). But this method has a number of disadvantages (dependence of the spectrogram from the window width and the amount of window overlap), so the method of "continuous" wavelet transform was additionally used, which was calculated through FFT (for analytically specified wavelets, for example Morlet) (comparative review in [14]). Representations were used in visualization: Magnitude: $\sqrt{R^2+I^2}$, PSD SSA (Surface Integral Sum Squared Amplitude Power): $2(R^2+I^2)$, decibels (dB): $10\log_{10}(R^2+I^2)$, where R – real part, I – imaginary part, of wavelet transform.

3. Results of observations of ionospheric scintillations of cosmic radio sources

The following sections discuss some results of the study features of the manifestation ionospheric scintillations of cosmic radio sources on geomagnetically disturbed and calm days. As shown in Figure 4 (22-24 Sep 2021), during the days of ionospheric storm development, the scintillation spectrum varies significantly from source to source, and even the same source 3C 274 has completely different types of scintillation.

It is worth noting that the band of periods 10-20 minutes corresponds to large-scale wave activity of the ionosphere, for example, the passage of acoustic (2-4 minutes) and gravitational waves (5-20 minutes). These waves arise not only in the *F*-layer of the ionosphere, but also in the *D*-layer (altitude about 100 kilometers), which is also evident from variations in the total electron content determined from properties of the GPS signal [15]. More details about ionospheric waves are described in the work

[16]. In the period band 5 minutes – 30 seconds, in mid-latitudes, quasi-periodic scintillations in the range 10-30 MHz appear infrequently, they are mainly recorded in circumpolar regions (for example, according to data from the Kilpisjärvi Atmospheric Imaging Receiver Array (KAIRA) [17]). In mid-latitudes, quasiperiodic ionospheric variations, their registration and study are significant scientific interest, since they are a consequence of the formation of a spatial periodic structure of ionospheric irregularities passing through the beam of the antenna array.

3.1 Cassiopeia A (3C 461)

Supernova remnant Cassiopeia A (3C 461) together with Cygnus A (3C 405) are the most powerful radio sources in the Northern Hemisphere sky in the decameter radio range and, accordingly, the most popular for research. Figure 5 shows examples of STFT spectrograms of source 3C 461 for Sep 27-28, 2021 (quiet geomagnetic field) and Jul 2, 2021 (weakly disturbed geomagnetic field). The example shows that even weak geomagnetic disturbances often lead to a shortening of the "period" of scintillations, from 24 seconds to 16 seconds. In general, this is often true for other sample sources as well. During strong magnetic storms, the "periods" of 3C 461 scintillations are shortened to 10 – 5 seconds. For 3C 461, quasi-periodic flux variations are sometimes recorded, with periods of several minutes. During some strong magnetic storms of 2022, quasi-periodic variations of about 1 minute or 30 seconds, and lasting 10 – 15 minutes, were recorded at a frequency of 20 MHz in both linear polarizations A and B.
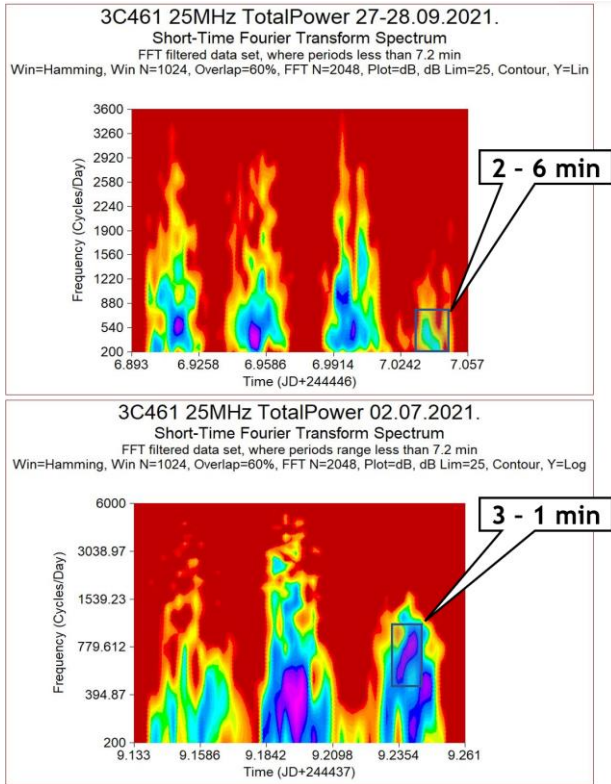
Figure 5: Examples of STFT spectrograms of source 3C 461 at a frequency of 25 MHz, obtained on Sep 27-28, 2021, quiet geomagnetic field (upper graph) and Jul 2, 2021, weakly disturbed geomagnetic field (lower graph), linear polarization A. Rectangles show events of quasiperiodic variations of radio flux of Cassiopeia A (the range of periods is shown by flags on the figure).
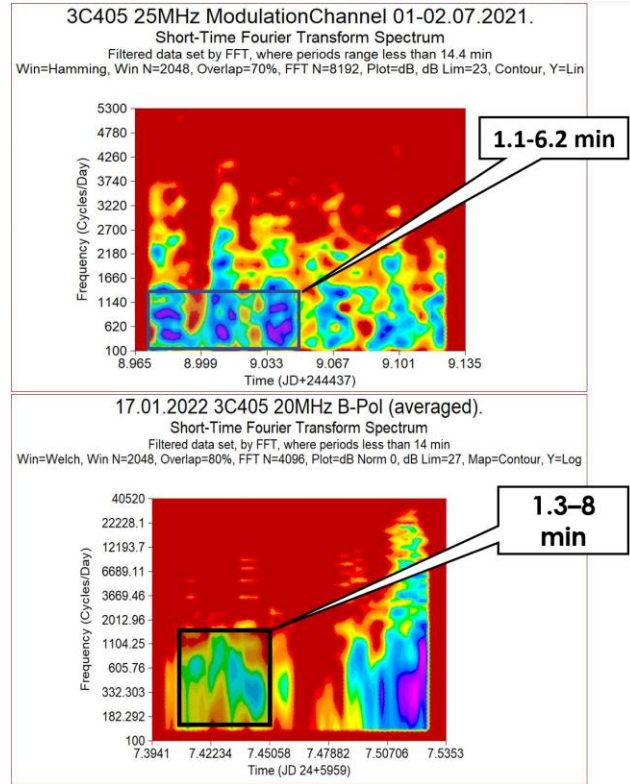

Figure 6: Examples of STFT spectrograms of source 3C 405 at a frequency of 25 MHz, weakly disturbed geomagnetic field, 1-2 Jul 2021 (top graph) and at a frequency of 20 MHz, magnetic storm, 17 Jan 2022 (bottom graph), linear polarization B. Rectangles on the graphs areas are highlighted quasi-periodic variations of the radio flux and flags mark the ranges of changes in the "periods" of oscillations.

3.2 Cyg A (3C 405)

The giant radio galaxy Cygnus A (3C 405) is one of the most popular radio sources for studying the ionosphere in the decameter radio range. The signal from it is powerful and at the same time almost free from noise and radio-interference. Ionospheric scintillations from this source are very intense and change rapidly over time, showing a complex time-frequency structure. Figure 6 shows examples of STFT spectrograms for the 3C 405 source at frequencies of 25 MHz (1-2 Jul 2021) and 20 MHz (17 Jan 2022). On 1-2 Jul 2021 there was a weakly disturbed geomagnetic field, and on 17 Jan 2022 there was a magnetic storm of medium intensity. During a magnetic storm, a significant change in the quasi-period of variations was noted from approximately 1.3 minutes to 8 minutes, increasing with time. During weak geomagnetic disturbances, short-lived "bursts" of quasi-periodic scintillations are sometimes recorded in a period band of approximately 1 – 6 minutes, as shown in this example. Also, at source 3C 405, during some magnetic storms, high-intensity and broadband scintillations of a noise-like appearance are observed, occupying a band of periods in the spectrogram, usually from 10 minutes to 4 seconds. In the sample of sources under study, a similar type of "noise-like" spectrogram was observed at source 3C 274.

3.3 Virgo A (3C 274)

Another giant radio galaxy 3C 274 (Virgo A) in the studied sample of radio sources is similar in properties to ionospheric scintillations to 3C 405, however, fewer quasi-periodic manifestations of scintillations were observed at this source. Scintillations are mostly noise-like and broadband (example in Figure 7). Observation sessions lasting several days, in 2020 and 2022, showed that the maximums of the FFT power spectra of 3C 274, during weak geomagnetic disturbances, lie in the range of 1 – 3 minutes or less. Rare quasiperiodic flux variations with periods from 30 seconds to 1 minute, and duration 5 – 12 minutes, corresponded to geomagnetic storms caused by geoeffective solar coronal mass ejections.

3.4 Taurus A (3C 144)

The radio source 3C 144 is one of the actively studied objects in decameter radio astronomy. The fact is that this powerful radio-bright object (the remnant of a supernova explosion) annually approaching the Sun on the celestial sphere (in June), shining through the quite dense layers of outflowing solar wind, which are called the supercorona. During this period, intense scattering of radio waves from
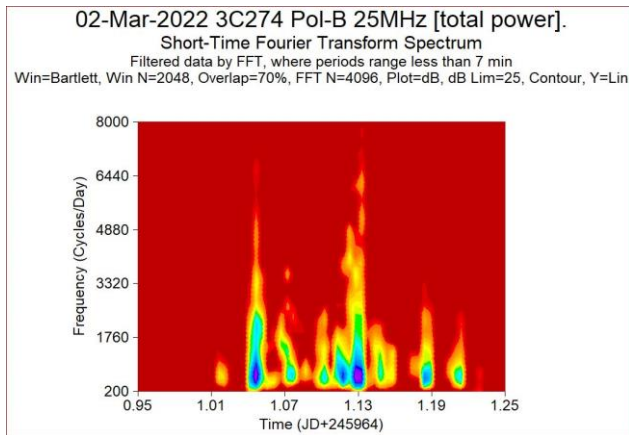
Figure 7: An example of a STFT spectrogram of source 3C 274, for a recording obtained on March 2, 2022 (weak geomagnetic disturbances) at a frequency of 25 MHz, polarization B. Noise-like broadband scintillations are clearly visible here.
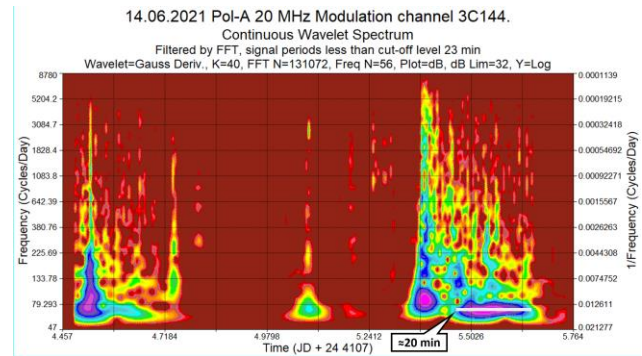

Figure 8: An example of extreme amplification of scintillations of the radio source 3C 144, at an angular approach to the Sun on June 14-15, 2021. Wavelet spectrogram at a frequency of 20 MHz, polarization A. In addition, on June 15, 2021, a quasiperiodic component of variability is visible with a period of about 20 minutes and a duration in several hours (marked with a flag in the figure).

source 3C 144 occurs on plasma clouds of the solar wind (interplanetary scintillation effect). However, this type of scintillations cannot be detected on the URAN-4 antenna array, because their period is on average about 1 second or less. But, besides this, the high turbulence of the supercorona plasma, caused by solar wind from flares, coronal mass ejections [18], provides complex effects on the radio signal of a source. An interesting effect was observed on June 14-15, 2021, when 3C 144 approached the minimum angular distance from the Sun. Figure 8 shows the wavelet spectrum of 3C 144. It can be seen that on June 14 and 15 there was an extreme increase in scintillation at 3C 144, while the rest of the sources from the observation session scintillated much weaker (almost "empty" spectrum between scans of 3C 144). The amplitude of scintillations 3C 144 was 4 times greater than the source 3C 461. This type of effect is discussed in more detail in the article [19].

The exact nature of this effect is not known, but is possibly related to coronal mass ejections or magnetized plasma clouds that may provide lens-like amplification to the observed radio emission. More details about such effects are described in the works [20, 21, 22, 23]. Variations in the radio-flux with a period of about 20 minutes are most likely have ionospheric origin, the passage of moving ionospheric irregularities or ionospheric waves [24]. Therefore, studying records of the annual passage of 3C 144 through the solar supercorona is always with scientific interest, and such observations continue to be carried out on the URAN-4 antenna array.

3.5 Perseus A (3C 84)

The radio source 3C 84 has the smallest flux in the decameter range from the studied sample of radio sources. However, there is minimal interference and distortion in the direction to this source, which makes it important for studying ionospheric disturbances at the URAN-4 location.

At the same time, the properties of 3C 84 ionospheric scintillations are somewhat different from other radio sources in the sample. The maximums of the FFT power spectra show that the main spectral power of the signals falls on the period range of 40 seconds – 1.5 minutes, on days of a quiet geomagnetic field. Figure 9 shows wavelet spectrograms of 3C 84 for Oct 9, 2020 (quiet geomagnetic field) and Apr 8, 2021 (weak geomagnetic disturbances). Noise-like scintillations are predominating. However, in a number of magnetic storms (Jun 12, 2021), fairly stable scintillations appear on the spectrograms with periods of about 50, 25, 16 seconds, which exist for 2 – 3 hours, and sometimes longer. On days of a quiet geomagnetic field, stable quasi-periodic variations are occasionally recorded with a period of about 1.5 minutes – 40 seconds, and a manifestation duration of 2 – 3 hours (23 Sep 2021). In comparison with other radio sources of the studied sample, 3C 84 has much less frequent variations of the radio-flux in the period band of 20 – 5 minutes.

3.6 Effects of a solar eclipse on radio noise levels

Interesting observations were obtained during the annular solar eclipse on June 10, 2021. It was not the Sun observed on the URAN-4 antenna, but the background cosmic noise at frequencies of 20 MHz, 25 MHz (the antenna beam was directed to the zenith). As a result, it turned out that the cosmic background on the day of the eclipse and the next day, June 11, 2021, showed noticeable noisy variations, more intensive than in the records of the cosmic background on June 8-9, 2021. Spectrograms of radio background recordings are shown in the figure 10.
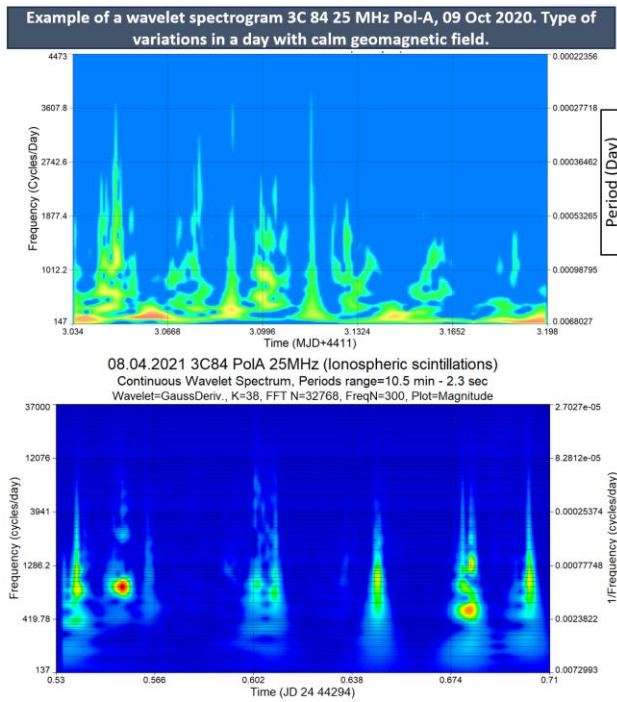
Figure 9: Example of wavelet spectrograms for source 3C 84. The top graph is a quiet geomagnetic field, Oct 9, 2020, frequency 25 MHz, polarization A. Many irregular bursts are visible, which is typical of ionospheric scintillations. Bottom graph – weak geomagnetic disturbances, 8 Apr 2021, frequency 25 MHz, polarization A. This is an interesting example of episodic noise-like scintillations of 3C 84.
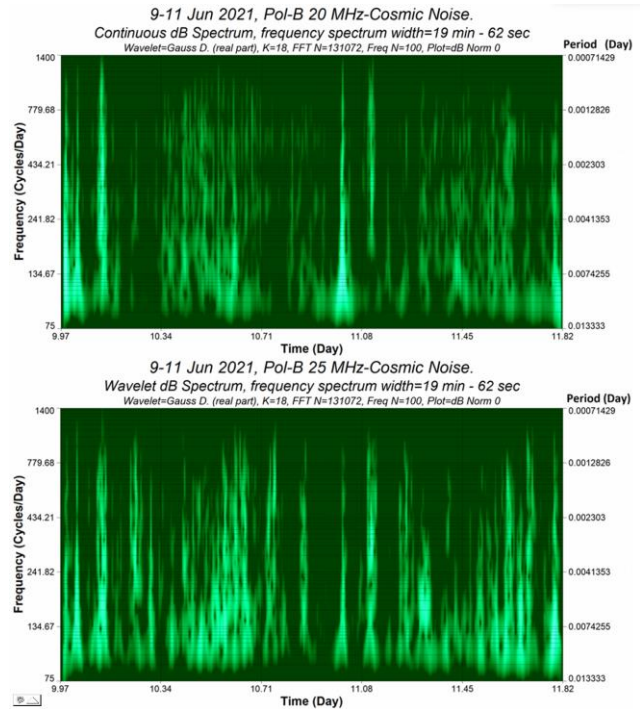
Figure 10: The figures show wavelet spectrograms of 20 MHz (upper plot) and 25 MHz (bottom plot) (B-linear polarization) obtained on June 10-11, 2021. The cosmic background records were cleaned of radio interference and additionally smoothed.

3.7 Interrelation with geomagnetic field variations in the Odessa anomaly zone

Increase in the intensity of radio noise was also observed by other researchers in different years of solar eclipses [25]. This is usually associated with a decrease in the electron concentration, a decrease in absorption in the ionosphere, which leads to an increase in the intensity of the noise received by the antenna [26]. However, it is interesting that the noise level on the day after the eclipse was still quite high. Also, there could be an increased level of radio-interference here. This is a very strange observational effect, showing that absorption in the ionosphere was still low even the day after the solar eclipse, but the reason for this effect is not clear. Something similar was observed in work [27] when the signal from a radio station increased during a solar eclipse, but a noticeable increase in the signal partially persisted the next day after the solar eclipse.

Analysis of observations showed, on June 8, 2021, two days before the partial solar eclipse visible in Ukraine, the amplitude of the sky background noise, when the antenna beam was set to the zenith, was much less than during the solar eclipse on June 10, 2021 and after it on June 11, 2021. Intensity of radio variations in the noise background, on a time scale of less than 8 minutes, was much weaker than on the day of the Solar Eclipse, and the low-frequency component of the spectrum (20.6 – 8 minutes) also has a lower intensity.

An important feature of the decameter radio range is that the observed scintillations of cosmic radio sources are almost completely (with the exception of some contribution of interplanetary scintillations for individual radio sources) determined by the dynamic processes of the ionosphere, under the influence of solar and geomagnetic activity. Seasonal-daily ionospheric effects during the solar activity cycle can be so great that they even exceed long-term intrinsic changes fluxes of the radio sources. For example, seasonal-diurnal effects significantly reduce the observed appearance of the secular decrease Cassiopeia A flux in the decameter range [28, 29, 30, 31]. This makes the decameter range especially interesting for searching and studying the interrelation between ionospheric scintillation and fast variations of geomagnetic induction, during magnetic disturbances and storms caused by different manifestations of solar activity.

Large magnetic anomalies in the Earth's lithosphere may have a quite high height of the anomalous field dome, which is recorded by satellites at altitudes of about 200-300 kilometers and even higher [32]. As is known, the most intense ionospheric scintillations are formed when radio waves pass through the F-layer of the ionosphere at altitudes of about 200 – 350 kilometers. Thus, large magnetic anomalies can influence the formation and structure of plasma irregularities, forming a special response of the ionosphere to solar activity events. In addition, local factors also play an important role in the

formation of geomagnetic variations in mid-latitudes [33]. Another important feature is the location of the seismically active Vrancea Zone in Romania, approximately 500 kilometers (290 km in a straight line) from Odessa. As is known, seismically active zones can produce ionospheric waves, including those with periods of tens of minutes (for example, [34]). Currently, this relationship is very poorly studied, especially in Europe, often due to the lack of large low-frequency radio telescopes in areas of magnetic anomalies. Therefore, the location of the URAN-4 antenna array in the area of the Odessa regional magnetic anomaly provides a unique opportunity to study this relationship. Conducted studies of short-period geomagnetic variations in the Odessa magnetic anomaly, which fall within the range of periods of observed ionospheric variations on the URAN-4 antenna array, showed a significant difference in their properties and structure from the variations that were observed at the magnetic station in the Kiev region (Dymer), where the geomagnetic field close to normal [35, 36, 37, 38]. In the summer of 2022, to conduct simultaneous observations of scintillations of radio sources and geomagnetic field disturbances, the LEMI-008 magnetometer of the Institute of Geophysics of the National Academy of Sciences of Ukraine was installed next to the URAN-4 antenna array. This makes it possible to obtain data for cross-spectral FFT analysis and identify similarities and differences in the development of magnetic storms based on geomagnetic and ionospheric variations. Fast geomagnetic variations are also induced in the ionosphere, but are associated with electric currents (field-aligned currents) and the interaction of the ionosphere and magnetosphere Earth. These include resonant geomagnetic variations [39]. Thus, ionospheric activity is studied as if in two dimensions. Preliminary results indeed showed a relationship between the prevailing periods of ionospheric scintillations of 30 seconds – 1 – 2 – 3 minutes and geomagnetic variations, using observations of the radio galaxies 3C 405 and 3C 274. An example of fast geomagnetic variations (*Bx* component of the geomagnetic field) with periods of about 1 minute and 30 seconds, shown in Figure 11. In winter wartime conditions, the magnetometer worked in the center of a magnetic anomaly in the basement on the territory of the Astronomical Observatory of the Odessa I.I. Mechnikov National University. On 22 Feb 2022 there was a weak geomagnetic storm, and on 13 Feb 2022 there was a magnetic storm of medium intensity. The variations shown in the example (falling in the period range Pc3 – Pc4 [40]), during weak and medium magnetic storms, were rarely observed in this form on spectrograms. Observations on URAN-4 of ionospheric scintillations of the radio galaxies 3C 405 and 3C 274, during weak and medium geomagnetic storms, showed that the average periods (in the bands of greatest spectral power) also had values of about 30 seconds and 1 – 2 – 3 minutes. But in general, since it was not possible to obtain complete sessions of simultaneous radio-magnetometric recordings, a clear relationship could not be detected. Solving this problem remained the goal of further work because placement a magnetometer in the summer 2023 in the Mayaki village, where URAN-4 is located.
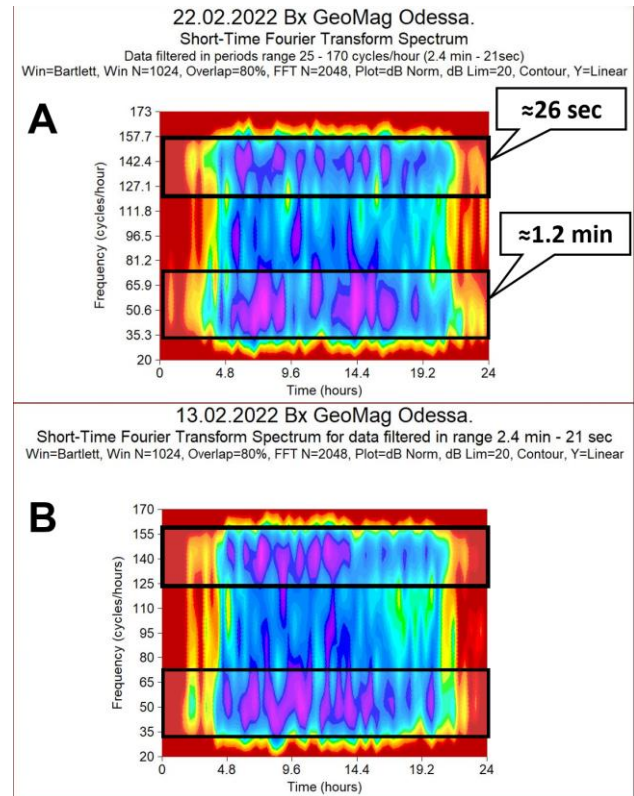

Figure 11: Examples of rapid variations in the geomagnetic field induction, component *Bx*, obtained at the Odessa Astronomical Observatory on 22 (top graph) and 13 (bottom graph) Feb 2022. Here you can see bands of quasi-regular oscillations falling in the pulsation range Pc3 (10 – 45 seconds) – Pc4 (45 – 150 seconds). Radio sources 3C 405 and 3C 274 often show similar average periods of ionospheric scintillations.

The interrelation between fast geomagnetic and ionospheric variations has been observed previously [41]. But these effects, in the case of using radio scintillations from cosmic radio sources, have been observed rarely, especially little information about the influence of geomagnetic anomalies on the correlation between ionospheric and geomagnetic variations. They are quite difficult to register, due to the fact that the decameter radio range is often very noisy. High-intensity geomagnetic variations appear in mid-latitudes most often during fairly strong magnetic storms (although there are exceptions), and moments of coincidence between the times of intense magnetic storms and the absence of radio-interference in the decameter range do not occur often. Nevertheless, long-term complex observations of the radio telescope-magnetometer system have great perspective. They will allow us to evaluate the response and contribution of the Odessa Magnetic Anomaly to the manifestation of space weather effects.

4. Conclusion

The creation of a joint measuring complex radio telescope – magnetometer IRA NASU and the Institute of Geophysics NASU (head of department M.I. Orlyuk)

provides a unique opportunity to identify the reaction and contribution of the Odessa magnetic anomaly to regional manifestations of space weather. Using a radiometer that was designed and manufactured by V.V. Galanin conducted many sessions of observing ionospheric scintillations of cosmic radio sources 3C 461, 3C 405, 3C 274, 3C 144 and 3C 84 near the Odessa Regional Geomagnetic Anomaly. The following main results were obtained:

1. A semi-automatic processing technique (data smoothing, removal of the sinusoidal trend of the antenna's beam pattern, bandpass filtering, to identify frequency bands of interest with intense ionospheric scintillation, calculation of STFT and wavelet spectrograms) was developed and tested on real radio sources observations on the phased array URAN-4 IRA NASU.

2. It is shown that the program for monitoring fluxes of powerful cosmic radio sources at URAN-4 provides an ionospheric response in the form of different amplitude, shape (quasi-periodic or noise), and changes in the frequency and phase of ionospheric scintillations over time. These indicators differ significantly for each of the radio sources in the sample during the development of geomagnetic disturbances.

3. The average periods corresponding to the bands of the highest spectral power for ionospheric scintillations in the URAN-4 location, usually vary in the range of 30 seconds – 1 – 2 – 3 minutes. On days of strong geomagnetic disturbances, scintillations periods can be shortened to tens of seconds or less.

4. Observations of ionospheric scintillations of radio galaxies 3C 405 and 3C 274 and comparison of them with fast geomagnetic variations (during magnetic storms) showed good agreement in the period bands corresponding to the Pc3 and Pc4 pulsations. In addition, coincidences are also observed for periods of about 3 minutes.

5. Mostly, ionospheric scintillations have an irregular, non-periodic structure. Nevertheless however, quasiperiodic variations are occasionally observed (more often during geomagnetic disturbances), with a change in period and amplitude in the range of 1 – 10 minutes.

6. Observations of changes in the intensity of background radio emission during the solar eclipse on June 10, 2021 at frequencies of 20 and 25 MHz showed an increase in background radio noise both during the eclipse and on the following day, June 11, 2021.

7. In the period band of 10–20 minutes, quasiperiodic variations of the radio flux predominate, probably associated with wave activity of the ionosphere (acoustic-gravity waves, moving ionospheric irregularities) caused by external influences. A possible contribution to these processes is the proximity of the Vrancea seismically active zone in Romania.

8. An important result of this work was the successful application of a new technique for processing ionospheric scintillation observations of the entire set of observed sources under the monitoring program. This allows us to significantly expand the list of scientific tasks in which the URAN-4 antenna array can be used. Among these tasks is the organization of comprehensive radio astronomy and magnetometric research together with foreign partners from the Ventspils International Radio Astronomy Center in Latvia) and the University of Oulu in Finland (Sodankyla Geophysical Observatory).

References

1. Vasilyev R., Globa M., Kushnarev D., Medvedev A., Ratovsky K.: 2017, ArXiv, https://doi.org/10.48550/arXiv.1702.01966
2. Cander L.R. Ionospheric Irregularities and Waves. In: Ionospheric Space Weather. Springer Geophysics, 2019. Springer, Cham. https://doi.org/10.1007/978-3-319-99331-7_7
3. Bovkoon V.P., Zhouck I.N.: 1981, *Astrophys. & Space Sci.*, **79**, 165.
4. Warwick James W.: 1964, *Radio Science J.*, **68D**, No. 2, 179.
5. Galanin V.V., Komendant V.H., Yasinski V.V.: 2021, *Odessa Astron. Publ.*, **34**, 74.
6. Galanin V.V., Lytvynenko O.A., Derevyagin V.G., Kravetz R.O.: 2018, *Odessa Astron. Publ.*, **31**, 128.
7. Gorbynov A., Sukharev A., Ryabov M., Bezrukovs V., Orbidans A.: 2021, *Galaxies*, **9**, No. 2, 30.
8. Hannibal H. Madden: 1978, Anal. Chem., **50**, No. 9, 1383.
9. Breaz Nicoleta: 2004, *Acta Universitatis Apulensis 7*, ResearchGate https://www.researchgate.net/publication/237262065
10. Garimella, Rao Veerabhadra: 2017, A Simple Introduction to Moving Least Squares and Local Regression Estimation. United States, Web ver. doi:10.2172/1367799
11. Tipton Carl: 2022, *Johnson Matthey Technol. Rev.*, 2022, **66**, No. 2, 169.
12. Hassani H., Thomakos D.: 2010, *Statistics and its Interface*, **3**, 377.
13. Allen J.: 1977, *IEEE Transactions on Acoustics, Speech, and Signal Processing*, **25**, Iss. 3, 235.
14. Wang Yun, He Ping: 2023, *RAS Techniques and Instruments*, **2**, Iss. 1, 307.
15. Lay Erin H., Shao Xuan-Min, Kendrick Alexander K., Carrano Charles S.: 2015, *J. of Geophys. Research: Space Physics*, **120**, Iss. 7, 6010.
16. Zawdie Kate, Belehaki Anna, Burleigh Meghan et al.: 2022, *Front. Astron. Space Sci.,* **9**, 1.
17. McKay-Bukowski Derek, Vierinen Juha, Virtanen Ilkka I.: 2015, *IEEE Transactions on Geoscience and Remote Sensing*, **53**, Iss. 3, 1440.
18. Yadav Vipin K.: 2016, *Universal Journal of Physics and Application*, **10**, Iss. 6, 193.
19. Galanin V.V., Derevjagin V.G., Kravetz R.O.: 2012, *Odessa Astron. Publ.*, **25**, Iss. 2, 186.
20. Gosling J.T.: 1975, *Rev. of Geophys.*, **13**, Iss. 3, 1053.
21. Vlasov V.I.: 2013, *Geomagnetism and Aeronomy*, **53**, Iss. 2, 137.
22. Bothmer V., Schwenn R.: 1998, *Ann. Geophysicae*, **16**, 1.
23. Galanin V.V., Derevjagin V.G., Kravetz R.O.: 2013, *Odessa Astron. Publ.*, **26/2**, 243.
24. Munro G.H.: 1950, *Proc. of the Royal Soc.*, **202**, Iss. 1069, 208.
25. Bhattacharya R., Nag A., Guha R., Bhoumick A., De S., Bhattacharya A.B.: 2010, *Indian Journal of Physics*, **84**, 1587.

26. Bossolasco M., Elena A.: 1962, *Geofisica pura e applicata*, **51**, 155.

27. Chandra H., Sharma Som, Lele P.D., Rajaram G., Hanchina A.: 2007, *Earth, Planets and Space*, **59**, 59.

28. Guglya L., Ryabov M., Panishko S., Sukharev A.: 2012, *Odessa Astron. Publ.*, **25**, Iss. 2, 207.

29. Ryabov M.I., Panishko S.K., Guglya L.I.: 2011, *Odessa Astron. Publ.*, **24**, 159.

30. Ryabov M.I., Serokurova N.G.: 1998, *Inform. Bull. of the Ukrainian Astron. Association*, **12**, 93.

31. Ryabov M.I., Serokurova N.G.: 1993, *Astron. & Astrophys. Trans.*, **4**, No.1, 29.

32. Kotsiaros S.: 2020, In: *Encyclopedia of Solid Earth Geophysics* /Gupta H.K. (eds). Encyclopedia of Earth Sciences Series, Springer, Cham. https://doi.org/10.1007/978-3-030-10475-7_276-1

33. Chen Chieh-Hung, Lin Jing-Yi, Gao Yongxin, Lin Cheng-Horng: 2021, *J. of Geophys. Res.: Solid Earth*, **126**, Iss. 3, e2020JB021416

34. Afraimovich E.L., Perevalova N.P., Plotnikov A.V., Uralov A.M.: 2001, *Ann. Geophysicae*, **19**, 395.

35. Ryabov M.I., Sukharev A.L., Orlyuk M.I., Sobitnyak L.I., Romenets A.A.: 2019, *Radiophys. and Radioastron.*, **24**, No. 1, 68.

36. Sobitnyak L.I., Ryabov M.I., Orlyuk M.I., Sukharev A.L., Romenets A.O., Sumaruk Yu.P., Pilipenko A.A.: 2020, *Radiophys. and Radioastron.*, **25**, No. 4, 324.

37. Sukharev A.L., Orlyuk M.I., Ryabov M.I., Romenets A.A.: 2018, *Radiophys. and Radioastron.*, **23**, No. 2, P. 116-127

38. Sukharev A., Orlyuk M., Ryabov M., Sobitniak L., Bezrukovs V., Panishko S., Romenets A.: 2022, *Astron. & Astrophys. Trans.*, **33**, Iss. 1, 67.

39. Klibanova Y.Y., Mishin V.V., Mikhalev A.V., Tsegmed B.: 2019, *Geodynamics & Tectonophysics*, **10**, Iss. 3, 673.

40. Menk F.W.: 1998, *J. Geomag. Geoelectr.*, **40**, 33.

41. Tedd B.L., Cole K.D., Dyson P.L.: 1989, *Planetary and Space Science*, **37**, Iss. 9, 1079.

42. Galanin V.V., Inyutin G.A., Kvasha I.M., Panishko S.K., Pisarenko Ya.V., Rashkovskij S.L., Ryabov M.I., Serokurova N.G., Tsesevich V.P., Sharykin N.K.: 1989, Kinem. & Phys. of Cel. Bod., **5**, 87.